Speckle Visibility Spectroscopy and Variable Granular Fluidization

P. K. Dixon[1,2] and D. J. Durian[1]

[1]*Department of Physics & Astronomy, University of California, Los Angeles, California 90095, USA*
[2]*Department of Physics, California State University, San Bernardino, California 92407, USA*

(Received 20 December 2002; published 8 May 2003)

We introduce a dynamic light scattering technique capable of resolving motion that changes systematically, and rapidly, with time. It is based on the visibility of a speckle pattern for a given exposure duration. Applying this to a vibrated layer of glass beads, we measure the granular temperature and its variation with phase in the oscillation cycle. We observe several transitions involving jammed states, where the grains are at rest during some portion of the cycle. We also observe a two-step decay of the temperature on approach to jamming.

DOI: 10.1103/PhysRevLett.90.184302 PACS numbers: 45.70.Mg, 78.35.+c, 81.05.Rm

A wealth of spectacular phenomena occur when granular materials are subjected to vertical vibration [1,2]. Shallow layers exhibit period doubling and pattern formation; deep layers exhibit heaping, convection, and logarithmically slow compaction. It is relevant to ask: What grain-scale physics causes this intriguing macroscopic behavior? Since the driving is generally at high amplitude but low frequency, the dynamics vary across the oscillation cycle. At first, the grains are jammed [3,4], completely at rest in some random packing configuration. When the downward acceleration exceeds $-g$, the grains are launched upward from the plate. The layer expands as the grains collide and move about randomly. Soon they crash back into the bottom plate and pick up energy from this impact. Finally, they come to rest after rattling away energy by inelastic collisions. This approach to jamming can be accompanied by clustering and "inelastic collapse," a finite time singularity where the collision rate diverges and the collision length vanishes [5,6]. This regime is especially significant because granular hydrodynamics [7–9] and statistical mechanics, extended to an athermal system, both break down.

Unfortunately, the above sequence has not been experimentally accessible. Because of multiple light scattering, video imaging is restricted to dilute granular gasses or surface behavior [10]. Even then, the spatial resolution becomes larger than the collision length as the grains come to rest. This limitation also holds for magnetic resonance imaging [11,12], x-ray microtomography [13], and positron emission particle tracking [14]. Furthermore, none is fast enough to capture the high collision rates when the grains are barely fluidized. By contrast, diffusing-wave spectroscopy (DWS) [15] is a dynamic light scattering (DLS) [16] method that applies to bulk granular media. It has superior spatial and temporal resolution and can be extended to unsteady dynamics [17]. However, it is based on temporal correlation functions, implicitly assuming that all times are statistically equivalent; therefore, it is not appropriate for periodic or aging systems. Altogether, the leading probe of dynamics in vibrated 3D granular systems currently is an NMR technique, where individual grains in a small highly fluidized sample were tracked to within about 150 μm and 1.4 ms [12].

In this Letter, we introduce a new DLS technique and use it to study grain dynamics across the oscillation cycle. The resolution is limited by the wavelength of light and by the speed of a fast CCD camera. Taking advantage of multiple light scattering, we achieve a resolution of $\approx$ 10 nm and ≈ 50 μs. With this advance, we unlock regimes where the grains barely move. In particular, we observe three dynamic transitions: the onset of fluidization, where the acceleration amplitude just exceeds g; a jamming transition, where the grains crash into the plate and then come to rest; and a transition to continuous fluidization, where the grains do not jam at any point during the cycle. In contrast, the NMR study of Ref. [12] was conducted far above this point, where granular hydrodynamics is applicable in the bulk. Our transitions all involve a jammed state, and therefore cannot be captured by granular hydrodynamics. Since our observations quantify the microscopics that underlie a host of intriguing phenomena, they present a theoretical challenge.

Our granular system consists of 780 ± 35 μm diameter glass beads, approximately 12 layers deep in a 10×10 cm^2 box with a flat transparent bottom, vertical walls, and an open top. This is mounted on a shake table, which in turn is leveled on an optical bench. Two three-axis accelerometers monitor the quality and peak acceleration, $a_\circ \equiv \Gamma g$, of the vertical sinusoidal oscillations. All data are taken at frequency $f = 10$ Hz. We define the phase to be $\phi = 0$ when the plate is at height $z = 0$ and moving upward. Properly leveled, we observe no discernible heaping, pattern formation, or convection across the range of amplitudes studied, $0 < \Gamma < 2.2$.

To measure grain motion, we introduce a method that we call "speckle visibility spectroscopy" (SVS). As shown in Fig. 1(a), we illuminate the grains from above with a ≈ 1 cm diameter beam of a 100 mW frequency-doubled Nd-YAG laser ($\lambda = 532$ nm). Photons perform a

random walk with transport mean free path of ≈ 4 grains. Since the sample is 12 layers deep, about $\frac{1}{3}$ of the photons reach the bottom plate, and the rest are backscattered after a few events. The backscattered light forms a speckle pattern in the far field, which we detect using a digital line scan CCD camera (Basler-160: 1024 pixels, 8 bit deep), and no intervening optics except a 532 nm filter. The sample-CCD distance is ≈ 20 cm, such that the speckle size is comparable to the pixel size (10 μm). Therefore, as the grains move and the speckle pattern changes, large intensity fluctuations occur at each pixel. For the speckle pattern to be visible, however, the exposure time of the CCD must be short compared to the time scale for speckle fluctuations. If the exposure time is longer, then the speckle blurs out and the same average intensity is recorded at each pixel. This is the essence of SVS. It is illustrated qualitatively in Fig. 1(b) by the space-time plot of speckle vs phase during the cycle. When the grains are at rest on the plate, the speckle is clearly visible. When the grains are fluidized, the speckle is blurry. The speckle is least visible just after impact, where rapid grain motion is excited by the sudden injection of energy. This is reminiscent of "laser speckle photography," where the absence of speckle in a laser-illuminated scene indicates motion [18,19]. And it is similar to even earlier work, where the intensity distribution at a single speckle was considered vs integration time [20].

The key measurable quantity in SVS is the variance of intensity across the pixels. For an exposure duration T, each of the N pixels reports a time-integrated intensity, $S_{i,T} = \int_0^T I_i(t)dt/T$. The ensemble-averaged intensity moments are computed as $\langle I\rangle_T = \sum_{i=1}^N S_{i,T}/N$, $\langle I^2\rangle_T = \sum_{i=1}^N S_{i,T}^2/N$, etc. If there are enough speckles, then the former is independent of T and the subscript may be dropped. By contrast, $\langle I^2\rangle_T$ depends on T and indicates the visibility of the speckles to the extent that it exceeds $\langle I\rangle^2$. To quantify visibility on a scale of 0–1, we define a normalized variance:

$$V_2(T) \equiv [\langle I^2\rangle_T/\langle I\rangle^2 - 1]/\beta. \quad (1)$$

The factor $1/\beta$ is roughly the number of speckles per pixel and is determined experimentally by measuring the system at rest. Figure 1(c) shows an example of $V_2(T)$ vs phase during the cycle, for a fixed exposure of $T = 100$ μs. It is closer to 0 when the grains are moving rapidly, and closer to 1 when the grains are coming to rest.

To relate the variance to grain motion, note that Eq. (1) involves *ensemble* averages, rather than time averages. Therefore, the Siegert relation [16] holds, giving $\langle I^2\rangle_T \equiv \langle \int_0^T \int_0^T I_i(t')I_i(t'')dt'dt''/T^2\rangle_i = \langle I\rangle^2 \int_0^T \int_0^T [1 + \beta|g_1(t' - t'')|^2 dt'dt''/T^2$. Here, β is the same as above, and $g_1(t)$ is the normalized electric field autocorrelation. Since $g_1(t)$ is even, the double integral simplifies and we arrive at the fundamental equation of SVS:

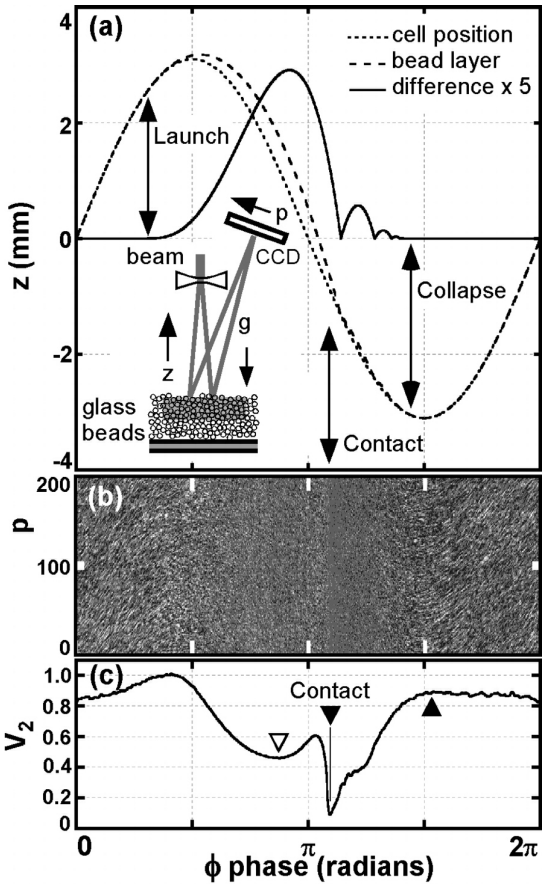

FIG. 1. (a) Theoretical position of the cell, bead layer, and their difference (5×) vs phase ϕ for a sinusoidally oscillated cell. The particular curves are for $\Gamma = 1.25$ and $f = 10$ Hz. For intuition, the bead layer is modeled as a slab with an effective coefficient of restitution; a value of $\epsilon = 0.5$ is used for the data shown. The inset shows the optical geometry. (b) A representative speckle image vs ϕ gathered by the linear CCD for $\Gamma = 1.25$, $f = 10$ Hz, and $T = 100$ μs. For clarity, only 200 of 1024 pixels are shown. (c) The averaged normalized variance V_2 of 300 full images versus ϕ for the above settings.

$$V_2(T) = 2\int_0^T (1 - t/T)|g_1(t)|^2 dt/T. \quad (2)$$

The variance is thus a weighted average of $|g_1(t)|^2$ over the exposure time T. Both functions are 1 at short times, and 0 at long times. Given $g_1(t)$ from SVS measurements, the scattering site motion may then be deduced by standard DLS practice. For random ballistic motion of average speed δv, the theory of DWS for backscattered light gives $g_1(t) = \exp(-\gamma t)$ with $\gamma = 4\pi\delta v/\lambda$ [15]. The corresponding variance is

$$V_2(T) = 2[\exp(-2\gamma T) - (1 - 2\gamma T)]/(2\gamma T)^2. \quad (3)$$

At short times, the initial decay is linear: $V_2(T) \approx 1 - \frac{2}{3}\gamma T$; at long times, it is a power law: $V_2(T) \approx 1/(\gamma T)$. The heavy weighting in Eq. (2) near $t = 0$ slows the decay, aiding in the measurement of fast processes.

We now return to Fig. 1, where the grains are vibrated at $f = 10$ Hz and $\Gamma = 1.25$, and exploit our SVS method. Three representative phases in the cycle are marked by triangles in the $V_2(100\ \mu s)$ data in Fig. 1(c): where the grain motion is most rapid both in midflight and after impact and where the grain motion ceases. For each of these three events, we show $V_2(T)$ vs T in Fig. 2(a). All data tend toward 1 (0) at short (long) times, as expected, where the speckle is most (least) visible. The actual dynamic range of our data is limited by two effects that are specific to our experiment (not the SVS method). First, for exposures faster than $\approx 50\ \mu s$, our 100 mW laser produces a signal that is a small fraction of the 0–255 range of the CCD. Therefore, the distribution of intensities is binned coarsely, which systematically distorts the variance. This limitation could be reduced by a brighter laser. Second, the macroscopic motion of the system contributes to the variance, becoming significant for $T \to \infty$ and/or $V_2 \to 1$. In particular, even if the grains are at rest, the speckles form a static pattern that washes as a whole across the CCD pixels. This "speckle wash" can be seen as a swirling in the space-time plot of Fig. 1(b).

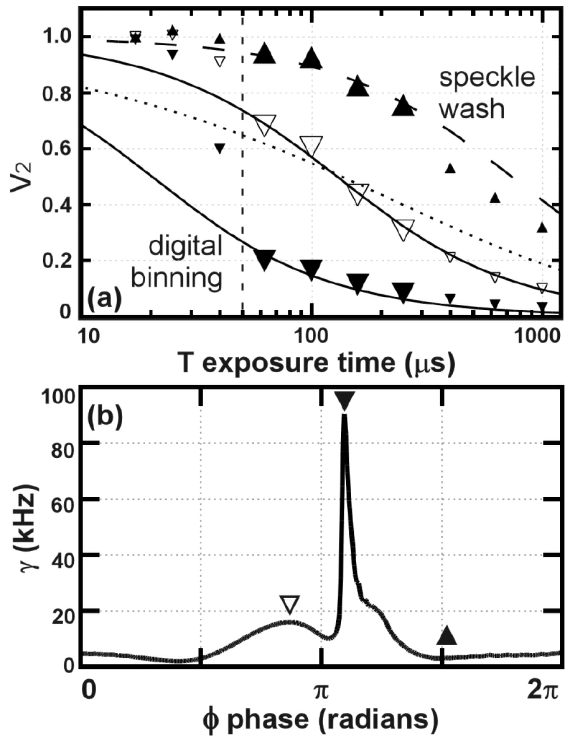

FIG. 2. (a) Variance V_2 vs exposure time T for $\Gamma = 1.25$ and $f = 10$ Hz at three phases ϕ. The symbols correspond to the markers in Fig. 1(c). The solid and dashed curves are single parameter fits to the data denoted by the larger symbols, using Eq. (3). The data fit by the dashed curve represent the effect of speckle wash alone, since the grains are at rest on the plate. The dotted curve assumes diffusive grain motion, $g_1(t) = \exp(-\sqrt{\gamma t})$, and gives a poor fit. (b) Fitted rates vs phase.

The reliable portion of the variance data in Fig. 2(a) compares well with Eq. (3), as shown by the curves. The form of the decay is therefore consistent with expectation: the grains appear to undergo random ballistic motion with some average fluctuation speed δv. For granular materials, the kinetic energy associated with δv is called the granular temperature; it is directly proportional to the decay rate $\gamma = 4\pi\delta v/\lambda$. Results for γ are shown in Fig. 2(b) as a function of phase in the cycle. The grains "heat up" both in midflight and from impact. In both cases, they lose energy through inelastic collisions. About $\frac{1}{5}$ cycle (20 ms) after impact, the grains lose their energy and come to rest in a jammed state. Because of speckle wash, however, γ does not decay to zero but rather to a readily identifiable baseline. To our knowledge, this is the first measurement of the bulk granular temperature during the collapse. Since "heat" is injected by collision with the plate, there may be a vertical temperature gradient; this is averaged over, and sampled fairly uniformly [21], by the diffusely backscattered photons.

We now repeat the experiment versus Γ, at constant $f = 10$ Hz. A gray scale plot of γ is shown in Fig. 3 vs both Γ and ϕ. Effectively, this is a phase diagram denoting the relative fluidization of the medium at different forcing rates and at different points in the cycle. Several transitions can be observed. First, below $\Gamma = 1$, there is no fluidization at all. Above $\Gamma = 1$, the grains become fluidized for some portion of the cycle. In particular, the grains are launched from the plate when the instantaneous acceleration is $-g$, as denoted by a solid white curve. The dotted white curve denotes where the grains crash back down, assuming they undergo simple free fall. Sometime after the grains land, they lose their energy via collisions and jam. The onset of both jamming and unjamming depend on the driving amplitude. For $\Gamma > 1.6$, they merge together and the system undergoes a transition

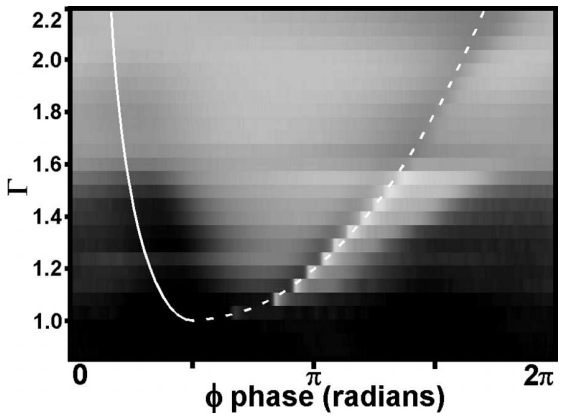

FIG. 3. Gray scale plot of decay rate γ, based on fits to Eq. (2), as a function of both peak acceleration Γ and phase ϕ in the oscillation cycle; black = 0, white = 120 kHz. The solid white curve indicates where the grains are launched, at an instantaneous acceleration of $-g$. The dotted white curve indicates when a free-fall object would land.

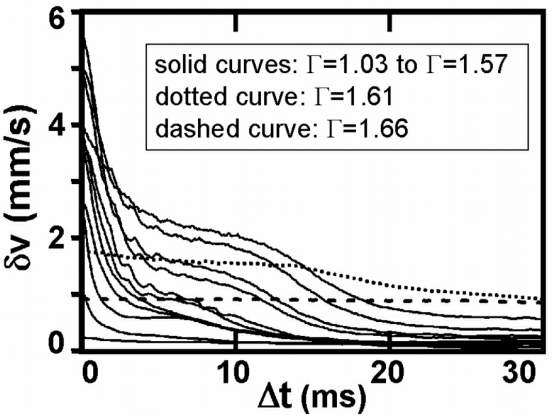

FIG. 4. Average fluctuation speed vs time after impact, extracted from Fig. 3, for different accelerations Γ. For the solid curves, all below the transition to continuous fluidization, δv increases monotonically with driving amplitude. Above the transition, δv never goes to zero and does not spike as strongly when the grains impact the plate.

to continuous fluidization. Though the grains never come to rest, their dynamics still vary throughout the cycle. As expected, the motion is fastest (slowest) just after (before) impact.

Both the process of jamming, and the nature of the transition to continuous fluidization, may be studied in terms of the fluctuation speed, δv, vs the time following impact, Δt. These data are extracted from Fig. 3 and displayed in Fig. 4. For amplitudes $1 < \Gamma < 1.6$, δv spikes at impact and then decays to a plateau after $\approx$ 2 ms; the initial decay rate appears to be independent of Γ. Following the plateau, δv decays to zero (within resolution set by speckle wash) as the grains jam up. This second decay is slower than the first. The temperature spike, the level of the plateau, and the duration of the plateau all increase monotonically with Γ. The impacts become progressively more violent, until suddenly at $\Gamma >$ 1.6 the plateau extends across the entire cycle and the grains never come to rest. The impacts are no longer as violent; instead, the grains stay fluidized and δv exhibits a smoother variation with time.

In conclusion, the use of area detectors for "multispeckle" dynamic light scattering is on the rise [22–25]. The general approach has been to autocorrelate each pixel and then to average the results afterwards, all in software. Our new method, speckle variance spectroscopy (SVS), is dramatically different and offers advantages in terms of both simplicity and applicability. In effect we have created a "speckle ensemble correlator" in which all averages are explicitly computed *ensemble* averages of a single exposure of the CCD camera; neither time averages, temporal autocorrelations, nor image storage are necessary. While the time resolution of prior methods is currently no better than $\approx$ 2 ms, we achieve $\approx 20\ \mu$s. More significantly, we can follow dynamics that *change* on equally rapid time scales. This unprecedented resolution allows us to capture the transition to continuous fluidization in Fig. 3 and the two-step decay of the granular temperature in Fig. 4. With a brighter laser, and better control of speckle wash, we are poised to study these and other granular dynamics in greater detail. SVS also opens a new window for the study of bubble rearrangements in coarsening foams, motion and aging in glassy suspensions, gelation, phase separation, and other phenomena that exhibit fast or quickly evolving nonstationary dynamics.

We gratefully acknowledge discussions with M. Giglio, P.-A. Lemieux, R. P Ojha, P. N. Pusey, T. Usher, and the support of NSF-0070329.

[1] H. M. Jaeger, S. R. Nagel, and R. P. Behringer, Rev. Mod. Phys. **68**, 1259 (1996).
[2] J. Duran, *Sands, Powders, and Grains: An Introduction to the Physics of Granular Materials* (Springer, New York, 2000).
[3] M. E. Cates, J. P. Wittmer, J. P. Bouchaud, and P. Claudin, Phys. Rev. Lett. **81**, 1841 (1998).
[4] A. J. Liu and S. R. Nagel, Nature (London) **396**, 21 (1998).
[5] I. Goldhirsch and G. Zanetti, Phys. Rev. Lett. **70**, 1619 (1993).
[6] Y. Du, H. Li, and L. P. Kadanoff, Phys. Rev. Lett. **74**, 1268 (1995).
[7] J. Jenkins and S. Savage, J. Fluid Mech. **130**, 187 (1983).
[8] V. Garzo and J. W. Dufty, Phys. Rev. E **59**, 5895 (1999).
[9] L. Bocquet, W. Losert, D. Schalk, T. C. Lubensky, and J. P. Gollub, Phys. Rev. E **65**, 011307 (2002).
[10] F. Rouyer and N. Menon, Phys. Rev. Lett. **85**, 3676 (2000).
[11] E. E. Ehrichs *et al.*, Science **267**, 1632 (1995).
[12] X. Yang, C. Huan, D. Candela, R.W. Mair, and R. L. Walsworth, Phys. Rev. Lett. **88**, 044301 (2002).
[13] G. T. Seidler *et al.*, Phys. Rev. E **62**, 8175 (2000).
[14] R. D. Wildman and D. J. Parker, Phys. Rev. Lett. **88**, 064301 (2002).
[15] D. A. Weitz and D. J. Pine, in *Dynamic Light Scattering*, edited by W. Brown (Clarendon, Oxford, 1993), p. 652.
[16] B. J. Berne and R. Pecora, *Dynamic Light Scattering* (Wiley, New York, 1976).
[17] P. A. Lemieux and D. J. Durian, Phys. Rev. Lett. **85**, 4273 (2000).
[18] A. Fercher and J. Briers, Opt. Commun. **37**, 326 (1981).
[19] Y. Aizu and T. Asakura, Opt. Laser Technol. **23**, 205 (1991).
[20] E. Jakeman, C. J. Olivier, and E. R. Pike, J. Phys. A **1**, 406 (1968).
[21] A. A. Cox and D. J. Durian, Appl. Opt. **40**, 4228 (2001).
[22] A. Wong and P. Wiltzius, Rev. Sci. Instrum. **64**, 2547 (1993).
[23] L. Cipelletti and D. A. Weitz, Rev. Sci. Instrum. **70**, 3214 (1999).
[24] D. Lumma, L. B. Lurio, S. G. J. Mochrie, and M. Sutton, Rev. Sci. Instrum.. **71**, 3274 (2000).
[25] V. Viasnoff, F. Lequeux, and D. J. Pine, Rev. Sci. Instrum. **73**, 2336 (2002).